Volumetric Reduced-Order Models of Zero-Net Mass-Flux Actuator

R. Messahel* and Y. Bury† and J. Bodart‡ and N. Doué§
Institut Supérieur de l'Aéronautique et de l'Espace (ISAE-SUPAERO), Université de Toulouse, 31055 TOULOUSE Cedex 4

In the framework of an optimization study based on a multi-objective optimization formulation, the consideration of optimization parameters such as the actuator location and the outlet design implies a re-meshing procedure that add complexity (even if the actuator is modeled with simple boundary conditions at the jet orifice exit since, locally, the re-mesh is still required). This strongly impacts the global computational cost, in particular if the considered geometry is complex. In this paper we propose an alternative method to model ZNMF synthetic jet actuators through the implementation of volumetric reduced-order models of ZNMF synthetic jet actuators as an additional source terms, in the form of body forces on given local control volumes corresponding to the actual locations of the actuators. This approach is promising as it allows to skip re-meshing procedures (velocity inlet boundaries or full synthetic jet actuator modeling) by directly plugging the volumetric source terms at appropriate locations and, consequently, save a considerable computational time during the optimization process.

I. Nomenclature

$\cdot_{ref}$	=	reference quantity
$\cdot_{amb}$	=	ambient quantity
$\cdot_{\infty}$	=	free-stream quantity
ρ	=	fluid's density
ρ	=	kinematic viscosity
τ	=	characteristic time scale
Γ	=	preconditioning matrix
Δx	=	characteristic cell length scale
Δt	=	time step
$\Delta\tau$	=	local pseudo-time step
σ	=	Von Neumann number
λ_{max}	=	maximum eigenvalue
c	=	chord length
CFL	=	Courant number
Cp	=	pressure coefficient
$d\mathbf{a}$	=	differential surface area
E	=	fluid's total energy
$freq$	=	membrane oscillation frequency
$\mathbf{F}$	=	inviscid flux vector
$\mathbf{G}$	=	viscous flux vector
H	=	fluid's total enthalpy
M	=	fluid's Mach number
p	=	fluid's pressure
$\mathbf{Q}$	=	primitive variables vector
$\mathbf{R}$	=	Residual vector

*Post-doctorate, Institut Supérieur de l'Aéronautique et de l'Espace (ISAE-SUPAERO), ramzi.messahel@isae.fr
†Associate professor, Institut Supérieur de l'Aéronautique et de l'Espace (ISAE-SUPAERO), y.bury@isae.fr
‡Associate professor, Institut Supérieur de l'Aéronautique et de l'Espace (ISAE-SUPAERO), j.bodart@isae.fr
§Research engineer, Institut Supérieur de l'Aéronautique et de l'Espace (ISAE-SUPAERO), n.doue@isae.fr

Re_c	=	Reynolds number based on the chord length
$\mathbf{S}$	=	source terms vector
t_f	=	simulation final physical time
T	=	fluid's temperature
$\mathbf{T}$	=	viscous stress tensor
$\mathbf{u}$	=	velocity vector
$U_{jet,max}$	=	peak velocity at the outlet of the SJA orifice
V	=	control volume
V_{roms}	=	ROM control volume
$\mathbf{W}$	=	conservative variables vector

II. Introduction

A. Context

The present study is carried in the framework of the European Clean Sky 2 Programme funded by the European commission under the project X-Pulse (cleansky 2 / LPA / X-Pulse GA 738172). It aims at developing innovative active flow control strategies, based on high frequency (few kilohertz) synthetic Zero-Net Mass-Flux (ZNMF) pulsed jets to mitigate the flow separation induced by UHBR power-plant installation on the suction side of the wing when the aircraft is operated at high angle of attack and low speed (take-off, initial climbing and landing). In the context of this research project, we consider complex industrial geometries (both for UHBR power-plant installation and synthetic jet actuator (SJA)) involving high Reynolds number, high pulsed jet frequencies (few kHz) and relatively high Mach numbers ($Ma \approx 0.3$). In the literature, most of the investigated ZNMF pulsed jet active flow control studies ([1]) consider canonical or simplified geometries, at relatively low Reynolds numbers and low excitation frequency (tens to hundreds Hertz).

In the framework of an optimization study based on a multi-objective optimization formulation, the influence of several SJA parameters is analyzed. These parameters are the actuation location, the number of ZNMF pulsed jets and their distribution, the outlet design, the pulsed jet momentum coefficient, the actuation frequency and the amplitude modulation. To optimize the ZNMF-based active flow control strategy, in the context of a meta-heuristic approach for instance, several numerical simulations have to be performed, resulting in a high CPU time consumption. This makes it hard to conciliate optimization studies and the use of high level turbulence modeling such as LES or DES to resolve the large range of turbulence length scales. Thus, RANS/URANS approaches that provide a more affordable computational cost are preferred. However, the consideration of optimization parameters such as the actuator location and the outlet design implies a re-meshing procedure that add complexity (even if the actuator is modeled with simple boundary conditions at the jet orifice exit since, locally, the re-mesh is still required) and a non-neglecting computational cost if the considered geometry is complex.

B. Objectives

Here we propose an alternative method to model ZNMF synthetic jet actuators (SJAs) through the implementation of volumetric reduced-order models (ROMs) of ZNMF synthetic jet actuators (SJAs) as an additional source terms, in the form of body forces on given local control volumes. In an optimization framework, the required re-meshing procedure (velocity inlet boundaries or full SJA modeling) can be avoided by plugging the volumetric source terms at appropriate locations and, consequently, save considerable computational time during the optimization process. In this study, we investigate the performance of unsteady ROMs to model the influence of ZNMF synthetic jet actuators in a flow subjected to an adverse pressure gradient. This adverse pressure gradient is promoted by a hump, as referenced in (CFDVAL 2004, case 3 [2]).

III. Methodology

The whole source term implementation strategy for actuator modeling relies in the use of the sponge boundary conditions technique [3–5], such that the flow variables are damped to a known reference solution through the addition of artificial volumetric source terms to the compressible Navier-Stokes equations at given control volumes.

Thus, in order to implement a robust volumetric ROM of ZNMF actuators, one may

- first, define the reference quantity to be set at the specified control volume,
- second, define the source term formulation to be added to the compressible Navier-Stokes equations.

For a given control volume, a constant-in-space reference quantity is applied. It is obtained by extracting the volume-averaged quantity over the control volume from a previous unsteady simulation including the full SJA model. In this study, we consider only the momentum quantity that is added as a momentum source term at the control volume location. As the Ma number is expected to be small enough, the influence of both the pressure field and the energy on the definition of the volumetric source terms can be considered as negligible. As such one can confidently mimic the action of the SJA and the induced ZMNF pulsed jet, through the sole momentum-based formulation. This allows to exclude the modeling of the actuator in the numerical simulation.

The RANS/URANS simulations are performed using the commercial code STAR-CCM+ with the coupled density-based solver on hexahedral mesh. A third-order MUSCL spatial scheme and implicit second-order temporal scheme are used for space discretization and time advancement, respectively. The $k-\omega$ SST-Menter turbulence model is used to model the unresolved scales.

A. Governing equations

For a given control volume V with differential surface area $d\mathbf{a}$, the Navier-Stokes (NS) equations are the following

$$\frac{\partial}{\partial t}\int_V \mathbf{W}dV + \oint \left[\mathbf{F}-\mathbf{G}\right].d\mathbf{a} = \int_V \mathbf{S}dV, \tag{1}$$

$$\underbrace{\mathbf{W}=\begin{bmatrix}\rho\\ \rho\mathbf{u}\\ \rho E\end{bmatrix}}_{\text{Cons. variables}},\quad \underbrace{\mathbf{F}=\begin{bmatrix}\rho\mathbf{u}\\ \rho\mathbf{u}\bigotimes\mathbf{u}+p\mathbf{I}\\ \rho\mathbf{v}H\end{bmatrix}}_{\text{Inviscid fluxes}},\quad \underbrace{G=\begin{bmatrix}0\\ \mathbf{T}\\ \mathbf{T}.\mathbf{u}+\dot{q}\end{bmatrix}}_{\text{Viscous fluxes}},\quad \underbrace{S=\frac{1}{\tau}\begin{bmatrix}\rho_{ref}-\rho\\ (\rho\mathbf{u})_{ref}-\rho\mathbf{u}\\ (\rho E)_{ref}-\rho E\end{bmatrix}}_{\text{Source terms}}, \tag{2}$$

where ρ, $\mathbf{u}$, p, H, E and $\mathbf{T}$ denote the fluid density, velocity, pressure, total enthalpy, total energy per unit mass, and viscous stress tensor, respectively.

S represents the considered "sponge zone" volumetric source terms formulation as described in [3–5], where ρ_{ref}, $(\rho\mathbf{u})_{ref}$, and $(\rho E)_{ref}$ are the quantities that we want to impose at control volumes located at the SJA slot exit location, and τ represents a characteristic time scale. The quantities $\rho_{ref}-\rho$ and $(\rho E)_{ref}-\rho E$ are set equal to zero (incompressible flow), and the reference momentum $(\rho\mathbf{u})_{ref}$ is interpolated from tables based on the record of one period time-averaged pulsed jet momentum. These tables are thus provided by a preliminary simulation that includes the full SJA. The source term formulation in Eq. (2) forces the solution to the user-specified reference solution at each time step using the adequate characteristic time scale τ.

B. Implicit time integration and dual time-stepping

In order to improve the time accuracy of the governing equations Eq. (1), a preconditioning matrix is introduced with a dual time-stepping approach to solve the unsteady flows, with inner iterations in pseudo-time as follows

$$\frac{\partial}{\partial t}\int_V \mathbf{W}dV + \Gamma\frac{\partial}{\partial \tau}\int_V \mathbf{Q}dV + \oint \left[\mathbf{F}-\mathbf{G}\right].d\mathbf{a} = \int_V \mathbf{S}dV, \mathbf{Q}=[p,\mathbf{u},T]^T, \tag{3}$$

where Γ and τ denote the preconditioning matrix and the pseudo-time variable, respectively (see [6]).

The additional second term introduces a local pseudo-time variation that is solved using the following second order implicit time marching approach such that it tends to 0 when $\tau\rightarrow\infty$:

$$Q^0 = Q_\tau, \tag{4}$$

$$\left[\Gamma+\frac{3}{2}\frac{\Delta\tau}{\Delta t}\frac{\Delta\mathbf{W}}{\Delta Q}\right]\Delta Q = -\alpha_i\Delta\tau\left[R^{i-1}+\frac{1}{2}\left(3\mathbf{W}^{i-1}-4\mathbf{W}^{t}+\mathbf{W}^{t-\Delta t}\right)+\underbrace{\mathbf{S}}_{constant\ in\ \Delta\tau}\right], \mathbf{S}=\frac{\mathbf{W}_{ref}-\mathbf{W}^0}{\Delta\tau} \tag{5}$$

where $\Delta Q = Q^i - Q^0$ and $R^{i-1}=\sum_{faces}\left(F(Q^{i-1})-G(Q^{i-1})\right)$, and the characteristic time scale in Eq. (2) is set to the local pseudo-time step $\Delta\tau(x)$ defined by the CFL condition

$$\Delta\tau(x) = min\left(\frac{CFLV(x)}{\lambda_{max}(x)}, \frac{\sigma\Delta x^2}{\nu(x)}\right) \tag{6}$$

Here CFL, $V(x)$, $\lambda_{max}(x)$, σ, Δx and $\nu(x)$ denote the dimensionless Courant number, the cell volume, the maximum eigenvalue of the system, the Von Neumann number, a characteristic cell length scale and the kinematic viscosity, respectively.

In the case of explicit time integration methods, the characteristic time scale in source term formulation is set to the physical time-step Δt.

C. Numerical implementation

The following steps summarize the numerical procedure to implement volumetric source terms in order to model ZNMF actuators:

1) Definition of the control volume $V_{roms}(x)$ where the volumetric ROMs is applied to model ZNMF actuators: in the present study, four to six layers of cells in the direction normal to the "effective" section of the SJA slot exit, *i.e.* without considering potential recirculation zones which may appear at the periphery of the outlet due to design effects (see Fig.1).
2) Run of a first unsteady simulation including the modeling of the full SJA cavity, and monitoring of the volume-averaged reference quantities over the control volume $V_{roms}(x)$.
3) Definition of the constant-in-space, volume-averaged source terms (Eq. (III.B)) over the control volume $V_{roms}(x)$), based on the monitored reference quantities : for incompressible flows, ρ_{ref} and $(\rho E)_{ref}$ are set equal to zero , and the reference momentum $(\rho \mathbf{u})_{ref}$ is set to the monitored quantity.
4) Application of the source terms at the cells within the control volume $V_{roms}(x)$.
5) Application of pressure outlet boundary conditions at $V_{roms}(x)$ boundary faces such that the velocity at the boundary face is extrapolated from the interior domain using reconstruction gradients.

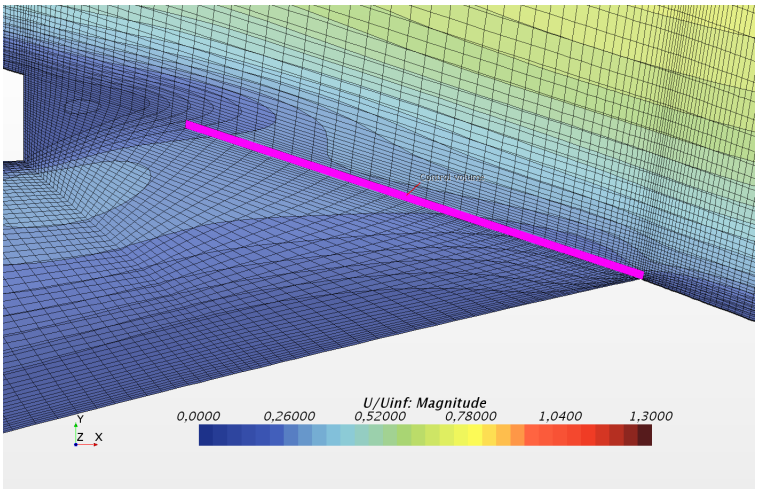

Fig. 1 Highlight of the control volume $V_{roms}(x)$ corresponding to a layer of four cells in the normal direction at the SJA slot exit limited to the flow effective section

IV. Numerical test: Flow over a hump model [2]

A. Problem description

The CFDVAL2004 workshop on synthetic jets and turbulent separation control (CFDVAL2004 [2]) that was held in March 2004 in Williamsburg, VA, proposed three test cases to assess different CFD methodologies and turbulence models to predict, in particular, flow fields induced by ZNMF synthetic jets and separation control. This workshop is an ideal benchmark for the validation of numerical methodologies as it is well-documented and also provides experimental data, guidelines and meshes for the CFD validation, as well as several detailed simulations in literature [7].

For the validation of the methodology, we consider the *'"Flow over a Hump Model"* third ZNMF oscillatory suction/blowing case with a membrane excitation frequency $freq = 138.5Hz$, a peak velocity at the outlet of the orifice during the blowing phase of cycle $U_{jet,max} = 26.6m/s$, a free-stream Mach number $M_\infty = 0.1$ and a Reynolds number

M_∞	U_∞	P_{amb}	T_{amb}	ρ_{amb}	μ
0.1	34.6 m/s	101325 $kg/(m.s^2)$	298 K	1.185 kg/m^3	$18.4e^{-6}$ $kg/(m.s)$

Table 1 Flow conditions

$Re_c = 0.936e^{+6}$ based on the chord length $c = 0.42m$. The start of the hump is located at the position $x/c = 0.0$. The flow conditions are given in Tab.1.

Velocity inlet, slip wall, pressure outlet and symmetry boundary conditions (BCs) are applied to the inlet and membrane, top wall, outlet and the side walls, respectively. The other boundaries are treated with no-slip BC. A sketch of the numerical setup is shown in Fig.2.

The computational time-step is set to $\Delta t = T/80$ where T denotes the synthetic jet period defined by $T = 1/freq$.

Several 2D grids are proposed on the NASA workshop website: structured *vs.* unstructured, with or without the SJA cavity, coarsened *vs.* refined, with or without an extended upstream region (up to $6.39c$ upstream of the hump) to match the boundary layer thickness with experimental data. In this study, we consider the extrusion of the coarse structured 2D grid #5 without the extended upstream region on $0.121c$ distance with a uniform grid points distribution. The top wall of the geometry has been adjusted to approximately account for side plate blockage found in the experiment. It corresponds to the slight section restriction located in the central part of the upper wall, above the hump (see Fig.2). The grids with and without the SJA contain approximately 2.0 and 1.7 millions cells, respectively. A sketch of the grid is shown in Fig.3.

In this study, we are interested on the robustness and ability of the volumetric ROMs approach to confidently predict the flow induced by ZNMF synthetic jets and their influence on the separation zone occurring in the wake of the hump, in regard to the results based on the numerical model including the SJA cavity. The numerical solution of the modeled SJA cavity setup is considered to be the reference solution for the validation of the volumetric ROM of ZNMF actuator setup.

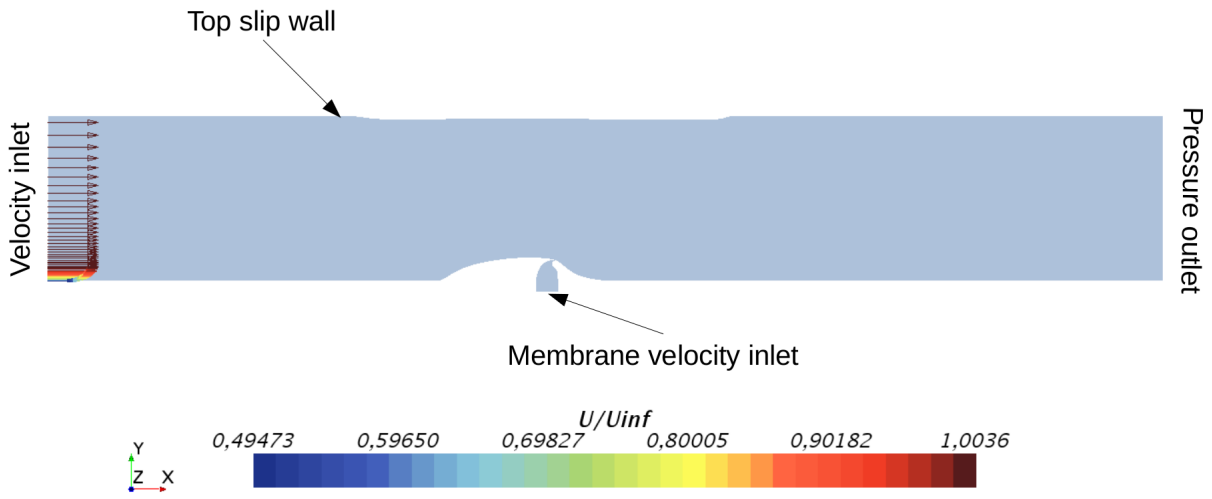

Fig. 2 Sketch of the numerical setup.

B. Results

In this paper, both simulations are run for a physical time $t_f = 13T$. The first eight periods are considered to evacuate the transient phenomena. The phase averages are performed on the last five periods of the computation.

For a qualitative comparison of the flow features between the SJA and ROM configurations, contours at the spanwise mid-plane of phase-averaged streamwise velocity, vertical velocity and velocity magnitude normalized by the free-stream velocity U_∞ are shown in Figures 456, respectively. Contours of the phase-averaged spanwise vorticity is illustrated in

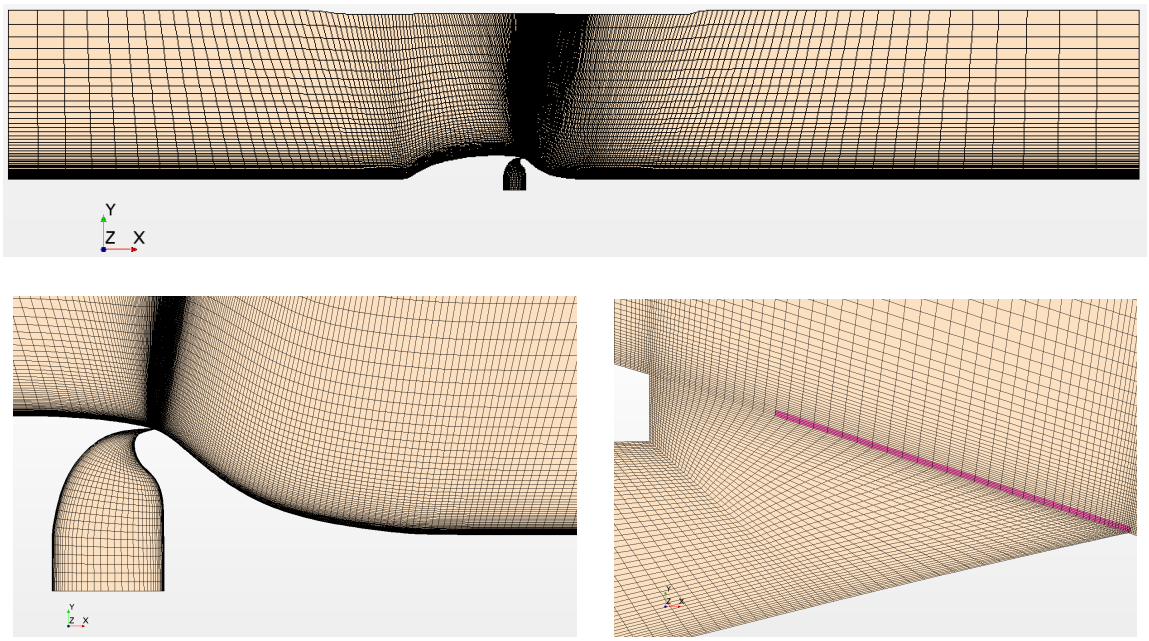

Fig. 3 Sketch of the 2D structured grid, with the monitored source term region highlighted in magenta.

Fig.7. Good agreements are found in terms of flow topology : synthetic-jet initial development and streamwise evolution under the influence of the outer flow. The synthetic jets and their induced vortices are well reproduced and advected by the ROM approach in comparison with the SJA approach. However, the detached vortices emanating from synthetic jets in the ROM configuration are slightly diffused when compared to SJA. Consequently, the mixing of the pulsed jet with the outer flow is reduced. This mitigated mixing is likely related to the definition of the ROM as proposed at that time of the study, which relies on a constant-in-space momentum vector profile at the ROM control volume in the source terms formulation. Indeed, the application of a constant volume-averaged quantity to all the cells within the ROM control volume imposes a mean volume flow and penalizes the promotion of the synthetic-jet vortex at the SJA slot exit as it probably slightly affects the close-to-outlet shear layers and resulting mixing process.

For a quantitative comparison of the flow features between the SJA and ROM configurations, pressure coefficient values and vertical velocity profiles at various locations ($x/c = 1.0$, $x/c = 1.1$, $x/c = 1.2$ and $x/c = 1.3$, see Figs.4,5,6 and 7 for details on the location of these profiles) are shown in Fig.8. The transcript of the instantaneous location of the pulsed jet-induced vortices is well predicted by both SJA and ROM approaches, as the peak of the pressure coefficients along the surface of the model depict good agreement. However one should notice the damping observed on the pressure coefficient curves of the ROM approach, as compared to the SJA approach downstream of the slot exit. As previously evoked, this damping may be promoted by the enforced mean volume flow at the ROM control volume which leads to a substantial weakening of the vortex enrollment.

V. Conclusion

In this paper, we have presented a robust volumetric Reduced Order Models of ZNMF actuator in replacement of the more standard approaches based on the modeling of the full SJA cavity or the application of velocity inlet boundary conditions at the exit orifice of the SJA.

The validation of the ROMs is performed on the *"Flow over a hump"* test case provided by the CFDVAL2004 workshop [2] through its comparison with a configuration that includes the modeling of the full SJA cavity. Qualitatively, good agreements is found in terms of flow topology and synthetic jet development and further advection by the external flow. However, the synthetic jets emanating from ROMs are moderately diffused in comparison with the SJA cavity full modeling approach, which affects the mixing properties of the jets.

An immediate extension to this work may consist in investigating different momentum vector profiles in the ROM control volume to promote the vortex structure formation at ROM control volume located at the SJA slot exit. Future

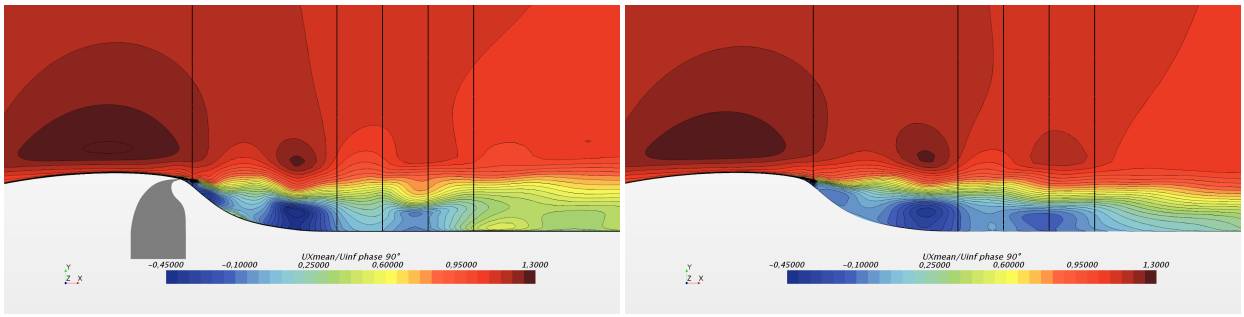

(a) Phase $\phi = 90°$

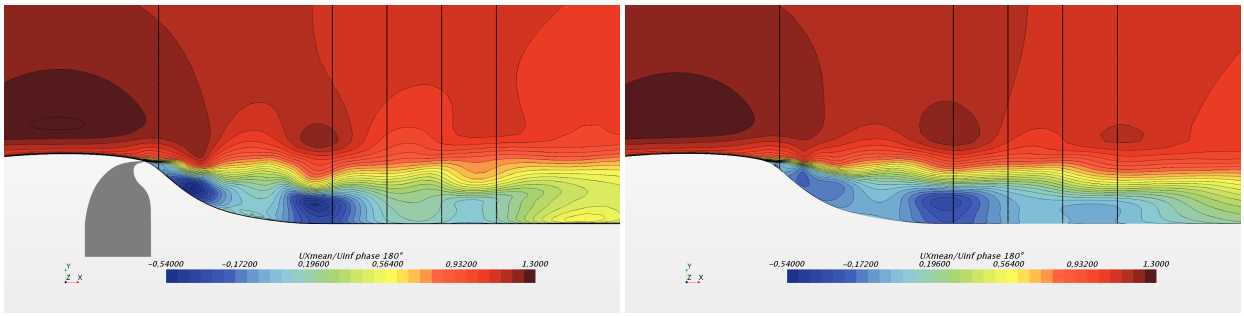

(b) Phase $\phi = 180°$

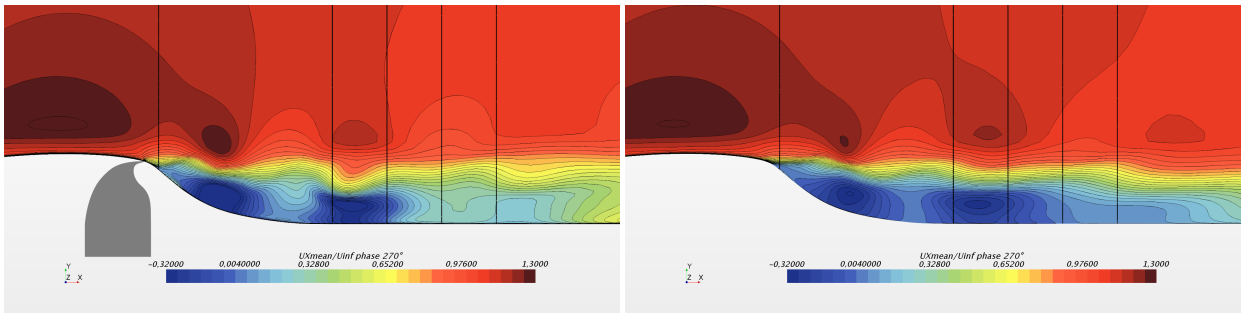

(c) Phase $\phi = 270°$

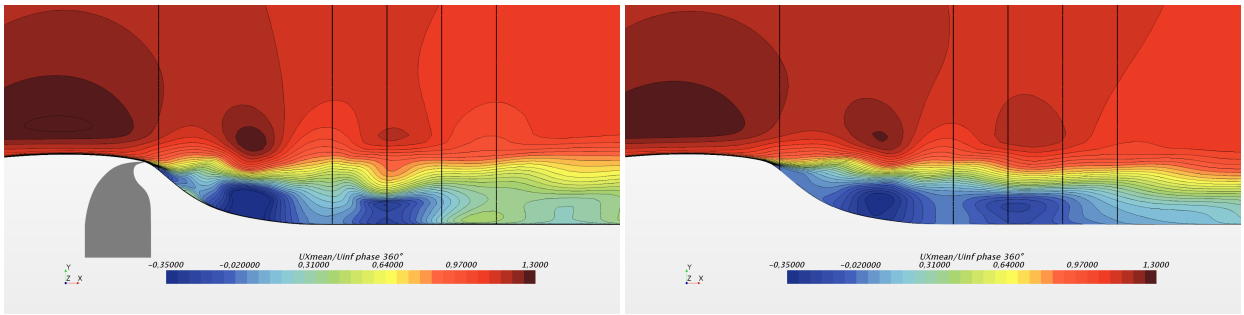

(d) Phase $\phi = 360°$

Fig. 4 Phase-averaged stream-wise velocity normalized by the free-stream velocity U_∞. Left : modeled SJA configuration. Right : ROM configuration. From left to right, the black transverse lines are positioned at $x/c = 0.6875$, $x/c = 1.0$, $x/c = 1.1$, $x/c = 1.2$ and $x/c = 1.3$.

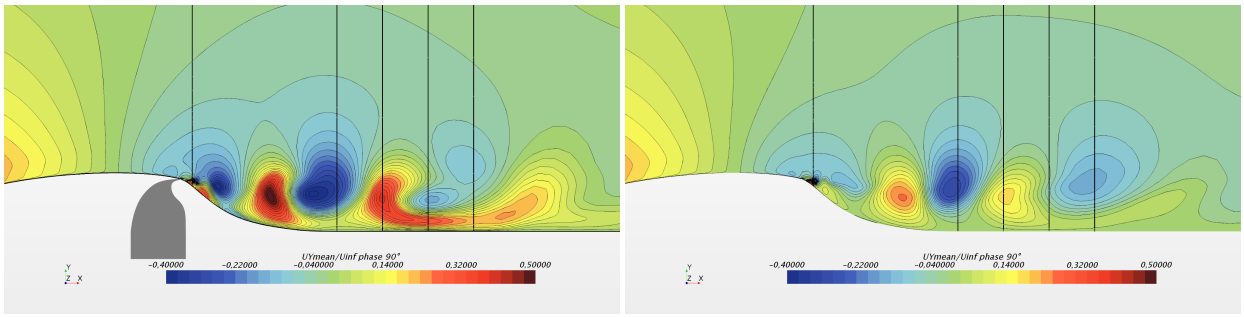

(a) Phase $\phi = 90°$

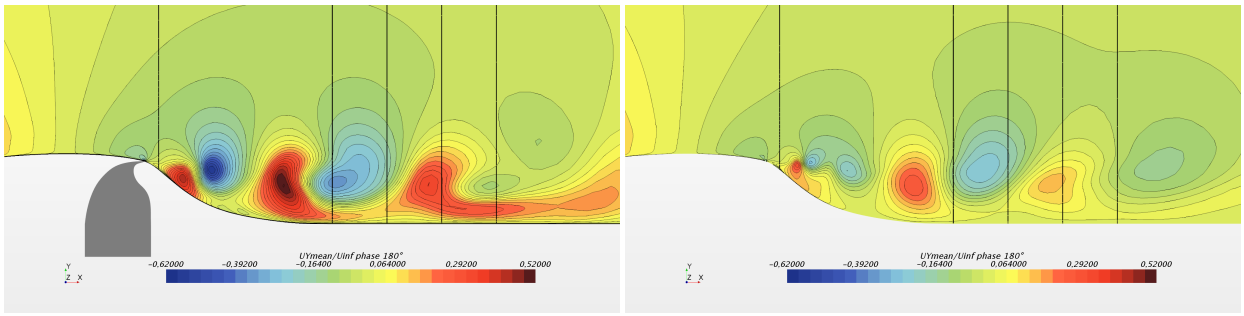

(b) Phase $\phi = 180°$

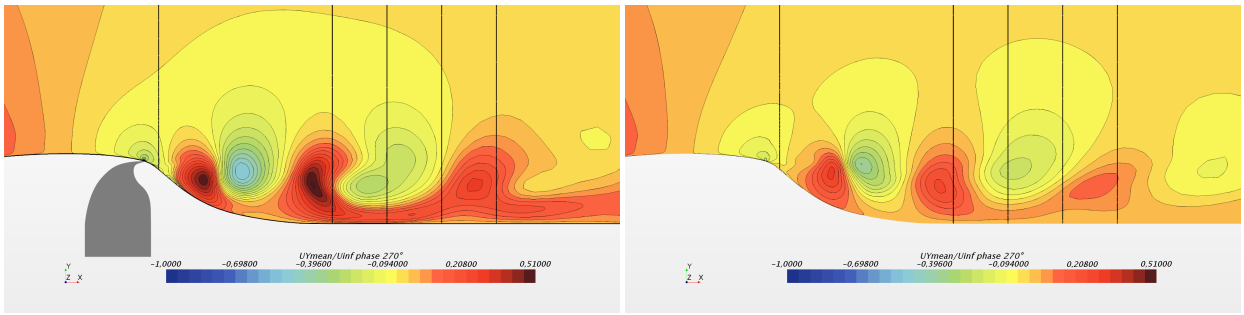

(c) Phase $\phi = 270°$

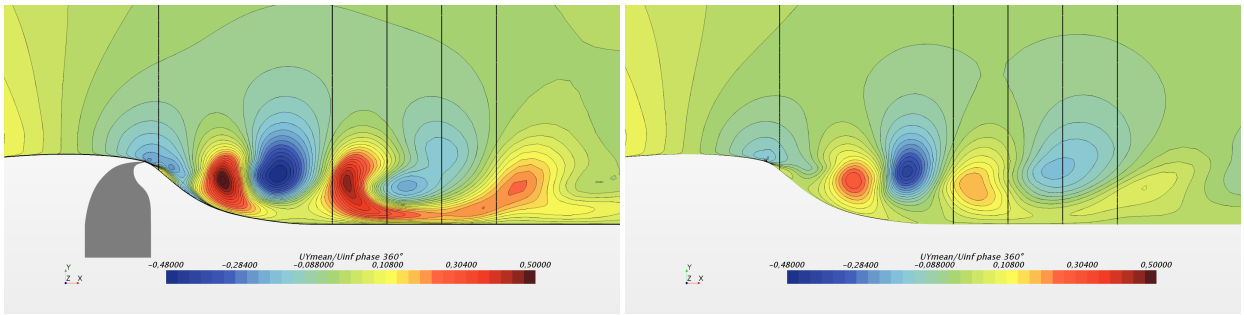

(d) Phase $\phi = 360°$

Fig. 5 Phase-averaged vertical velocity normalized by the free-stream velocity U_∞. Left : modeled SJA configuration. Right : ROM configuration. From left to right, the black transverse lines are positioned at $x/c = 0.6875$, $x/c = 1.0$, $x/c = 1.1$, $x/c = 1.2$ and $x/c = 1.3$.

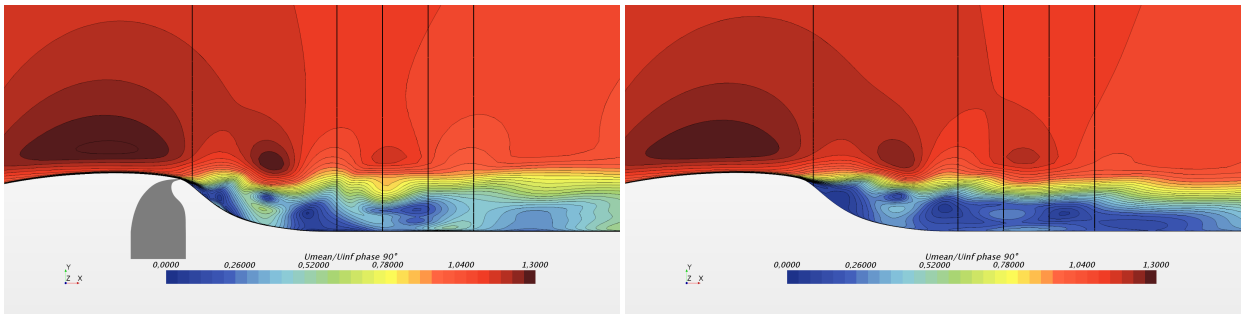

(a) Phase $\phi = 90°$

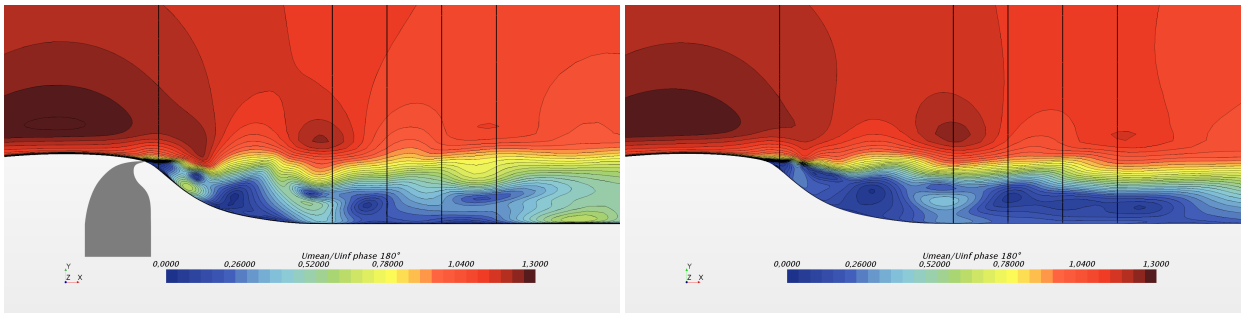

(b) Phase $\phi = 180°$

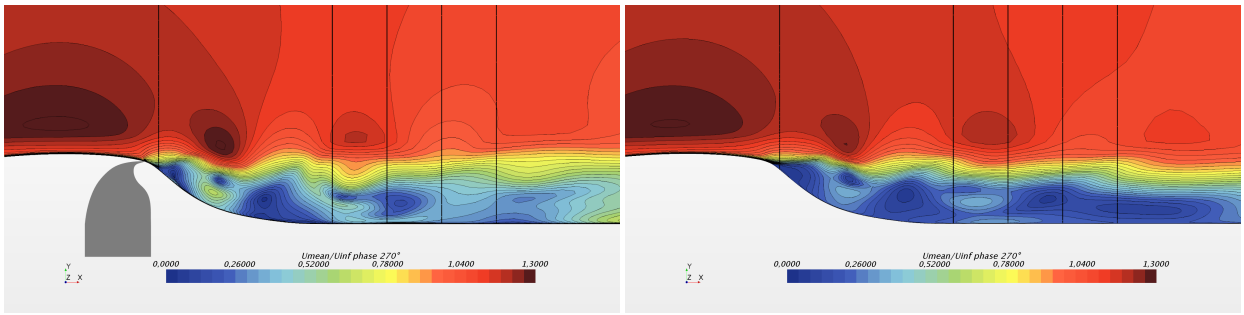

(c) Phase $\phi = 270°$

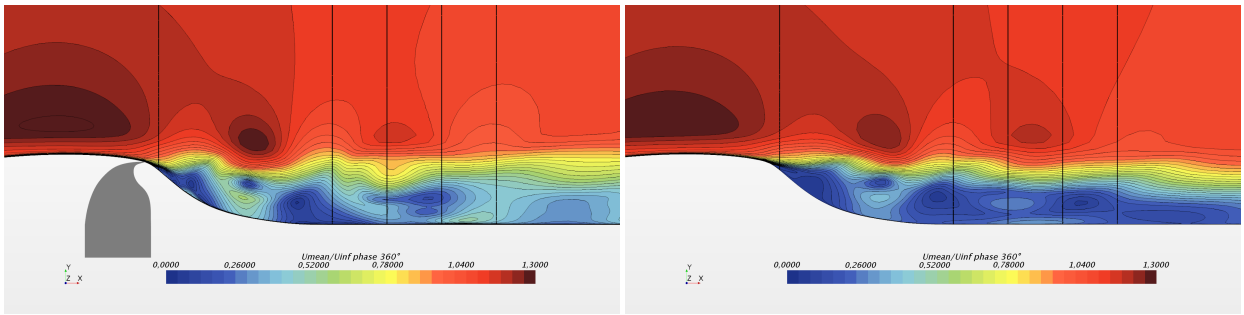

(d) Phase $\phi = 360°$

Fig. 6 Phase-averaged velocity magnitude normalized by the free-stream velocity U_∞. Left : modeled SJA configuration. Right : ROM configuration. From left to right, the black transverse lines are positioned at $x/c = 0.6875$, $x/c = 1.0$, $x/c = 1.1$, $x/c = 1.2$ and $x/c = 1.3$.

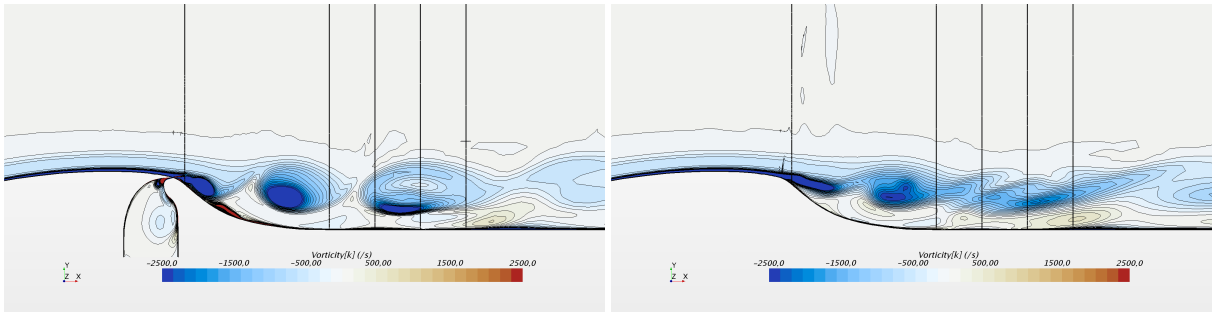

(a) Phase $\phi = 90°$

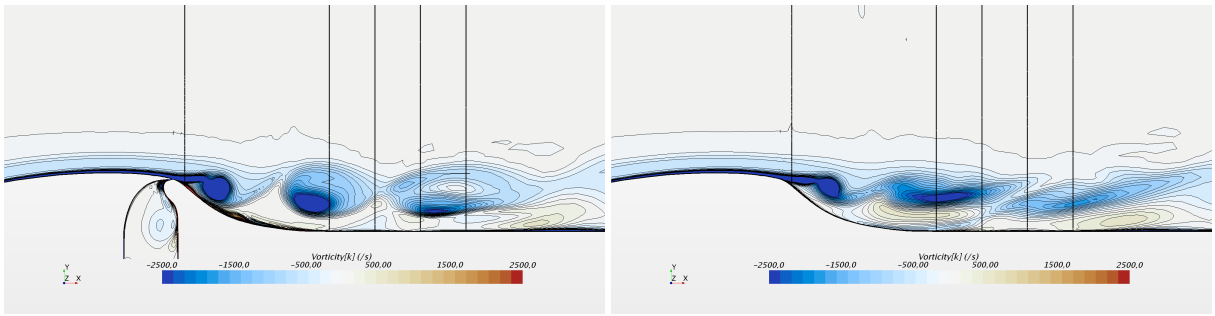

(b) Phase $\phi = 180°$

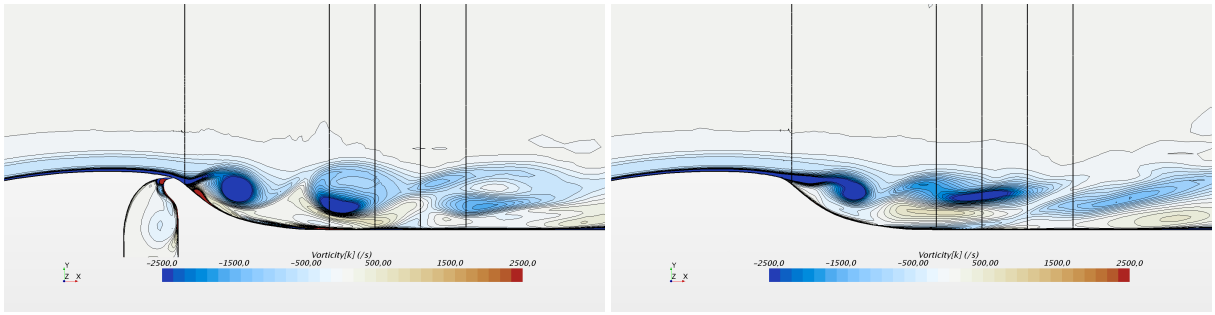

(c) Phase $\phi = 270°$

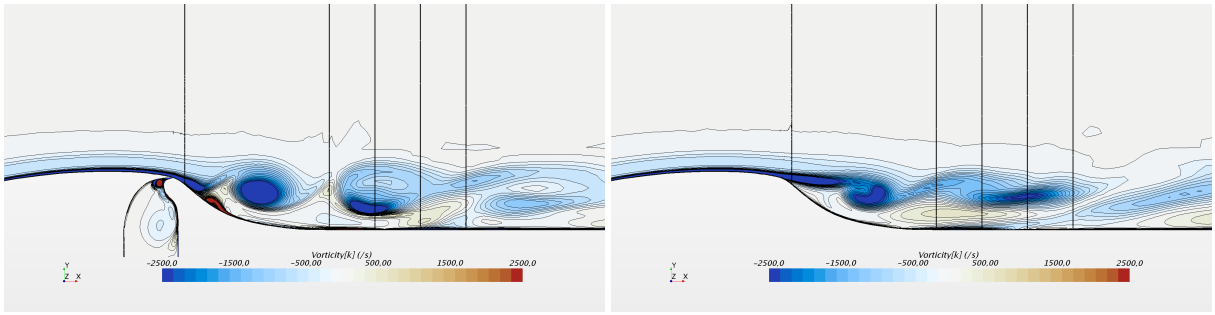

(d) Phase $\phi = 360°$

Fig. 7 Phase-averaged normal to plane vorticity. Left : modeled SJA configuration. Right : ROM configuration. From left to right, the black transverse lines are positioned at $x/c = 0.6875$, $x/c = 1.0$, $x/c = 1.1$, $x/c = 1.2$ and $x/c = 1.3$.

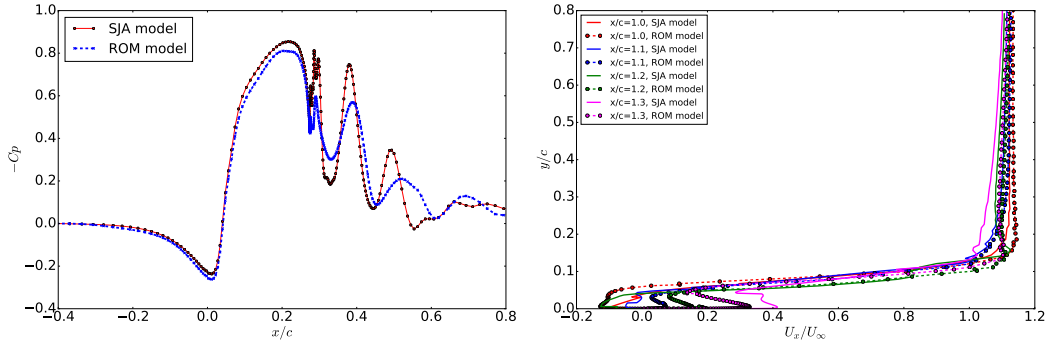

(a) Phase ϕ = 90°

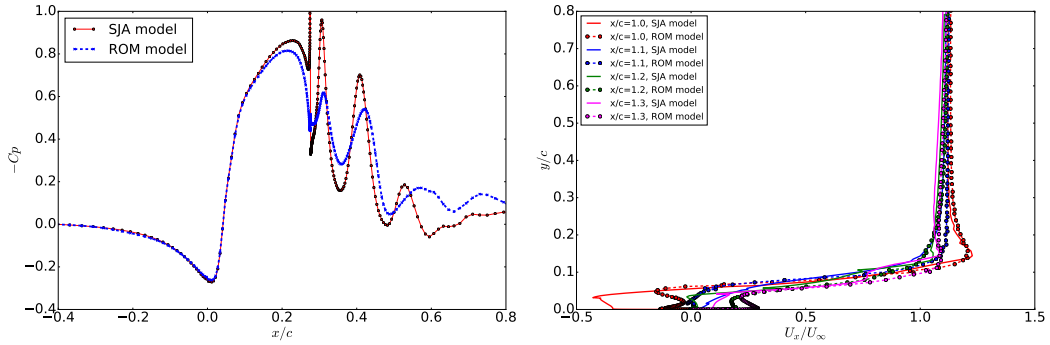

(b) Phase ϕ = 180°

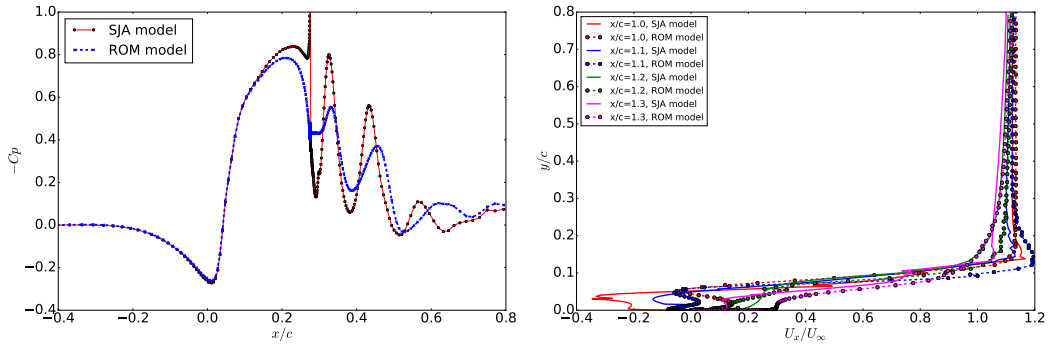

(c) Phase ϕ = 270°

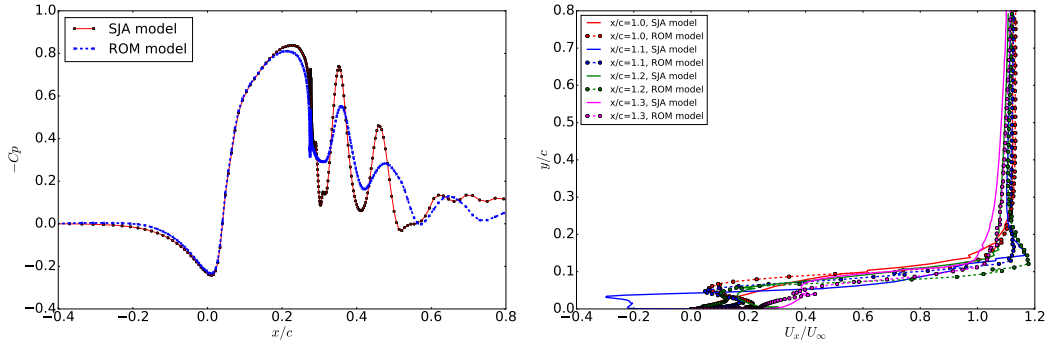

(d) Phase ϕ = 360°

Fig. 8 Left : Comparison of phase-averaged Cp vs. the dimensionless distance x/c between the SJA model (red) and the ROM model (blue). Right : Comparison of phase-averaged vertical velocity at various x/c locations between the SJA model (circles) and the ROM model (crosses).

works will be conducted in order to improve the robustness of ROMs and its application to more complex and realistic problems, in particular compressible flows at high Mach number with non-negligible thermodynamic variables in the source terms formulation.

Acknowledgments

The authors are grateful to the European commission for funding this research project from H2020 Programme for the Clean Sky 2 Joint Technology Initiative under Grant Agreement: cleansky 2 / LPA / X-Pulse GA 738172.

References

[1] Mohseni, K., and Mittal, R., *Synthetic jets: fundamentals and applications*, CRC Press, Hoboken, NJ, 2014. URL `https://cds.cern.ch/record/2019080`.

[2] Rumsey, C. L., Gatski, T. B., Sellers III, W. L., Vasta, V. N., and Viken, S. A., "Summary of the 2004 Computational Fluid Dynamics Validation Workshop on Synthetic Jets," *AIAA Journal*, Vol. 44, No. 2, 2006, pp. 194, 207. doi:10.2514/1.12957.

[3] Israeli, M., and Orszag, S., "Approximation of radiation boundary condition," *Journal*, Vol. 41, 1981, pp. 115, 135.

[4] Bodony, D., "Analysis of sponge zone for computational fluid mechanics," *Journal of Computational Physics*, Vol. 212, 2006, pp. 681,702.

[5] Mani, A., "On the reflectivity of sponge zones in compressible flow simulations," *Center for Turbulence Research, Annual Research Briefs*, 2010.

[6] Weiss, J., and Smith, W., "Preconditioning applied to variable and constant density flows," *AIAA Journal*, Vol. 33, 1995, pp. 2050,2057.

[7] NASA, "CFD Validation of Synthetic Jets and Turbulent Separation Control," , 2004. URL `https://cfdval2004.larc.nasa.gov/results.html`.